

A POPULATION OF NEUTRON STAR ULTRALUMINOUS X-RAY SOURCES WITH A HELIUM STAR COMPANION

YONG SHAO^{1,2}, XIANG-DONG LI^{1,2}, AND ZI-GAO DAI^{1,2}

¹Department of Astronomy, Nanjing University, Nanjing 210046, People's Republic of China; shaoyong@nju.edu.cn and
²Key laboratory of Modern Astronomy and Astrophysics (Nanjing University), Ministry of Education, Nanjing 210046, People's Republic of China; lixd@nju.edu.cn

Draft version October 16, 2019

ABSTRACT

It was recently proposed that a significant fraction of ultraluminous X-ray sources (ULXs) actually host a neutron star (NS) accretor. We have performed a systematic study on the NS ULX population in Milky Way-like galaxies, by combining binary population synthesis and detailed stellar evolution calculations. Besides a normal star, the ULX donor can be a helium star (the hydrogen envelope of its progenitor star was stripped during previous common envelope evolution) if the NS is accreting at a super-Eddington rate via Roche lobe overflow. We find that the NS–helium star binaries can significantly contribute the ULX population, with the overall number of about several in a Milky Way-like galaxy. Our calculations show that such ULXs are generally close systems with orbital period distribution peaked at ~ 0.1 day (with a tail up to ~ 100 days), and the helium stars have relatively low masses distributing with a maximum probability at $\sim 1M_{\odot}$.

Subject headings: binaries: general – stars: neutron – stars: evolution – X-ray: binaries

1. INTRODUCTION

An ultraluminous X-ray source (ULX) is an off-nuclear point-like source whose X-ray luminosity exceeds 10^{39} erg s⁻¹ (see Kaaret et al. 2017, for a review). It is generally believed that such a source is an X-ray binary (XRB) powered by accretion onto a compact object. An intermediate-mass ($10^2 - 10^5 M_{\odot}$) black hole (BH) with sub-Eddington accretion was firstly suggested by Colbert & Mushotzky (1999) to account for the observed X-ray luminosities. Several ULXs with extremely high luminosities, peaked at $\gtrsim 10^{41}$ erg s⁻¹, are thought to be promising intermediate-mass BH candidates (Farrell et al. 2009; Pasham et al. 2014). Alternatively the accretor is a stellar-mass compact object, accreting at a super-Eddington rate, as suggested by theoretical models (King et al. 2001; Begelman 2002; Poutanen et al. 2007) and observational features (Gladstone et al. 2009; Sutton et al. 2013; Walton et al. 2018). The mass of the compact object in M101 ULX-1 was dynamically measured to be in the stellar-mass BH range (Liu et al. 2013).

M82 X-2 is the first confirmed ULX hosting an accreting neutron star (NS) due to the discovery of X-ray pulsations (Bachetti et al. 2014). To date, quite a few of ULXs have been identified to host an NS accretor (see Table 1). In some cases, Be XRBs containing an NS can appear as ULX systems, as their peak X-ray luminosities¹ reach above 10^{39} erg s⁻¹ during outbursts (e.g., Tsygankov et al. 2017; Weng et al. 2017; Doroshenko et al. 2018). Theoretical models indicated that many unpulsed ULXs must actually contain an NS, because the ULX systems can be observed as pulsars only under rather special conditions (e.g., high spin-up rates) for the rotating NSs (King & Lasota 2016; King et al. 2017). Binary population synthesis (BPS) calculations

showed that a large fraction of ULXs are likely to host an NS rather than a BH accretor (e.g. Shao & Li 2015; Fragos et al. 2015; Wiktorowicz et al. 2017).

Until now, the properties of NS ULXs are still unclear. The detected X-ray luminosities can reach $\sim 10^{40} - 10^{41}$ erg s⁻¹ (e.g., Bachetti et al. 2014; Fürst et al. 2016; Israel et al. 2017a,b), meaning that the NS is accreting material at a rate of 2 – 3 orders of magnitude higher than its Eddington limit. These ULXs are highly variable sources, the luminosities in the faint phase can drop as low as $\lesssim 10^{37} - 10^{38}$ erg s⁻¹. This significant variability is proposed to be related to the interaction between the accreting material and the NS's magnetic fields which were estimated to be $\sim 10^9 - 10^{15}$ G (Bachetti et al. 2014; Ekşi et al. 2015; Dall'Osso et al. 2015; Kluźniak & Lasota 2015; Tong 2015; Karino & Miller 2016; Tsygankov et al. 2016; Chen 2017; Xu & Li 2017).

The nature of the donor stars in NS ULXs is not very clear. Based on the optical observations, the ULX donor of NGC 7793 P13 was determined to be a B19a star with a mass of 18–23 M_{\odot} (Motch et al. 2014). The donor mass of M82 X-2 was estimated to be greater than 5.2 M_{\odot} if assuming a 1.4 M_{\odot} NS companion (Bachetti et al. 2014). For the donor of NGC 5907 ULX-1, Israel et al. (2017b) suggested that it is likely to be a less-evolved massive star or a less-massive (super)giant. The optical observations with *HST* data still cannot confirm the donor nature of this ULX system (Heida et al. 2019). The donor mass of NGC 1313 X-2 was limited to be $\lesssim 12M_{\odot}$, provided that it is associated with a young star cluster in its vicinity (Sathyaprakash et al. 2019). In the source M51 ULX-7, Rodríguez Castillo et al. (2019) suggested that the donor star is an OB giant with mass $\gtrsim 8M_{\odot}$. Several investigations were performed to search for the ULX donors, but only a handful have been detected among hundreds of known ULXs (Roberts et al. 2008; Gladstone et al. 2013; Heida et al. 2014). As a result of the observational bias that favoring bright stars, the detected donors in NS

¹ Throughout this paper, the X-ray luminosity means the inferred luminosity for an assumed isotropic emission, even though the emission is not actually isotropic.

TABLE 1
 BASIC PROPERTIES OF THE ULX SYSTEMS WITH AN NS ACCRETOR, INCLUDING PEAK X-RAY LUMINOSITY L_{peak} , PULSAR'S SPIN PERIOD P_{spin} , BINARY ORBITAL PERIOD P_{orb} , DONOR'S MASS FUNCTION f_M , AND ESTIMATED DONOR MASS M_d .

Name	L_{peak} (erg s^{-1})	P_{spin} (s)	P_{orb} (days)	f_M (M_{\odot})	M_d (M_{\odot})
M82 X-2 (1)	2×10^{40}	1.37	2.51 (?)	2.1	$\gtrsim 5.2$
NGC 7793 P13 (2)	10^{40}	0.42	63.9		18–23
NGC 5907 ULX-1 (3)	10^{41}	1.13	5.3 (?)	6×10^{-4}	
NGC 300 ULX-1 (4)	5×10^{39}	~ 31.5		$\lesssim 8 \times 10^{-4}$	
M51 ULX-8* (5)	2×10^{39}				
NGC 1313 X-2 (6)	$\sim 10^{40}$	~ 1.5	< 4 (?)		$\lesssim 12$
M51 ULX-7 (7)	7×10^{39}	2.8	2	6.1	$\gtrsim 8$

* The compact object in the source M51 ULX-8 is believed to be an NS, since the detection of a likely cyclotron resonance scattering feature that produced by the NS's surface magnetic field.

References. (1) Bachetti et al. (2014). (2) Fürst et al. (2016); Israel et al. (2017a); Motch et al. (2014). (3) Israel et al. (2017b). (4) Carpano et al. (2018); Binder et al. (2018). (5) Brightman et al. (2018). (6) Sathyaprakash et al. (2019). (7) Rodríguez Castillo et al. (2019).

ULX systems tend to be luminous massive stars.

It is known that NS ULXs are binary systems in which the NS is being fed by the donor via Roche lobe overflow (RLOF) (e.g., Shao & Li 2015; Fragos et al. 2015). Modeling the evolution of NS X-ray binaries reveals that the mass transfer is dynamically unstable when the initial mass ratio of the donor star to the NS is larger than ~ 3.5 (Kolb et al. 2000; Podsiadlowski & Rappaport 2000; Tauris et al. 2000; Podsiadlowski et al. 2002; Shao & Li 2012). Such a binary will go into a common envelope (CE, see a review by Ivanova et al. 2013) phase, and the remnant system may be an NS–helium star binary if the progenitor donor has evolved off main-sequence prior to mass transfer (Bhattacharya & van den Heuvel 1991). The subsequent evolution of this binary can lead to the formation of a close system with a massive white dwarf (WD) orbited by a (partially) recycled pulsar (e.g. van den Heuvel & Taam 1984; Dewi et al. 2002; Tauris 2011). Binary evolution simulations reveal that the NS–helium star binaries are potential ULXs since the mass transfer can proceed at super-Eddington rates via RLOF (Wiktorowicz et al. 2015; Tauris et al. 2015). However, there is little attention on the formation and evolution of these ULX binaries in the literature. In this paper, we attempt to explore the properties of the NS ULXs with a helium star companion in Milky Way-like galaxies, including the parameter distribution of the binary systems and the number size of this ULX population. For comparison, we simultaneously provide the information of the NS ULXs with a normal star companion (see also Shao & Li 2015).

The remainder of this paper is organized as follows. In Section 2 we introduce the adopted methods, using the BPS code *BSE* (Hurley et al. 2002) to obtain the birthrate distribution of incipient NS binaries and the stellar evolution code *MESA* (Paxton et al. 2011) to model the binary evolutionary tracks. In Section 3, we present the calculated results and give some discussions. Finally we make a brief summary in Section 4.

2. METHODS AND CALCULATIONS

2.1. Generation of incipient NS binaries

An incipient NS binary is defined as a binary system containing either a normal star (NS–normal star) just after the NS formation, or a helium star (NS–helium star)

just after the CE evolution during which its hydrogen envelope is stripped by the NS. The subsequent evolution of incipient NS binaries may become ULX systems if the donor supplies its material to the NS at a super-Eddington RLOF rate. To obtain the birthrate distributions of the incipient NS binaries, we adopt the BPS code *BSE* originally developed by Hurley et al. (2002). With *BSE* we can simulate the evolution of a large number of binary stars with different initial parameters, i.e. the component masses and the orbital parameters. The evolutionary process is assumed to begin from a primordial binary containing two zero-age main-sequence stars. Modeling the evolution of a binary system is then subject to many factors, e.g. tides, stellar winds, mass and angular momentum transfer, asymmetric supernova (SN) explosions and natal kicks, and CE evolution. Some modifications in the code have been made by Shao & Li (2014), in the following we will introduce some key points.

During the evolution of a primordial binary, the primary star firstly evolves to fill its Roche lobe and supplies its envelope matter to the secondary star. If the secondary star accretes so rapidly that it gets out of thermal equilibrium and significantly expands to fill its own Roche lobe, then the binary goes into a contact phase (Nelson & Eggleton 2001). Therefore the mass transfer efficiency (the fraction of matter accreted onto the secondary star among the transferred matter) is an important factor that determining whether the primordial binary goes into a contact phase. When dealing with the evolution of the primordial binaries, Shao & Li (2014) built three mass transfer models with significantly different efficiencies. It is found that the rotation-dependent mass transfer model (in which the efficiency is assumed to be dependent on the rotational velocity of the secondary star) appears to be consistent with the observed parameter distributions of Galactic binaries including Be–BH systems (Shao & Li 2014), Wolf Rayet–O systems (Shao & Li 2016) and NS–NS systems (Shao & Li 2018). So we employ the rotation-dependent mass transfer model in our calculations. In this model, the accretion rate onto the rotating secondary is assumed to be the mass transfer rate multiplying a factor of $(1 - \Omega/\Omega_{\text{cr}})$, where Ω is the angular velocity of the secondary star and Ω_{cr} is its critical value (Petrovic et al. 2005; de Mink et al. 2009; Stancliffe & Eldridge 2009). Since accretion of a

small amount of mass can accelerate the secondary to reach its critical rotation (Packet 1981), the mass transfer efficiency can be as low as < 0.2 . As a consequence, the maximal initial mass ratio of the primary to the secondary stars for avoiding the contact phase can reach ~ 6 , and then a large number of the primordial binaries can experience stable mass transfer phases until the primary’s envelope is completely exhausted. The contact binaries are assumed to enter a CE phase if the primary star has evolved off main-sequence, otherwise they are assumed to merge into a single star (see e.g., de Mink et al. 2013; Shao & Li 2014).

If a binary system goes into the CE evolution, we use the standard energy conservation equation (Webbink 1984) to calculate the orbital decay during the spiral-in phase. The orbital energy of the embedded binary is used to expel the envelope. After CE evolution, the binary system is assumed to merge into a single star if the final separation leads to contact between the binary components, which will not contribute the ULX population. In the code, we use the results of Xu & Li (2010) and Wang et al. (2016) for the binding energy parameter of the donor envelope and take the CE efficiency to be 1.0^2 . Alternatively if the mass transfer in a binary proceeds stably without involving a CE phase, the donor envelope will be gradually stripped via RLOF. In the case of stable mass transfer, we simulate the binary orbital evolution by assuming that the ejected matter takes away the specific orbital angular momentum of the accretor. During the whole evolution, we use the prescription of Hurley et al. (2000) to treat the stellar wind mass losses, except for hot OB stars, for which we adopt the mass loss rates of Vink et al. (2001).

We assume that NSs are formed through either electron-capture or core-collapse SNe, the criterion suggested by Fryer et al. (2012) is used to distinguish them. In the *BSE* code, the helium core mass at the AGB base is used to set the limits for the formation of various CO cores (Hurley et al. 2002). If the helium core mass is smaller than $1.83M_{\odot}$, the star forms a degenerate CO core, and eventually leaves a CO WD. If the core is more massive than $2.25M_{\odot}$, the star forms a non-degenerate CO core, stable nuclear burning will continue until the occurrence of a core-collapse SN. Stars with core masses between $1.83M_{\odot}$ and $2.25M_{\odot}$ form partially degenerate CO cores. If such a core reaches a critical mass of $1.08M_{\odot}$, it will non-explosively burn into an ONe core. If in subsequent evolution the ONe core can increase its mass to $1.38M_{\odot}$, the core is believed to collapse into an NS through an electron-capture SN. It should be noted that the trigger of SN explosions is actually subject to big uncertainties, and binary evolution makes it more complicated (e.g., Podsiadlowski et al. 2004). During a SN explosion, the newborn NS will be imparted a natal

² Dewi & Tauris (2000) indicated that observations of the NS–WD binaries originating from a CE evolution are consistent with the CE efficiency of $\lesssim 1$. When dealing with the post-CE binaries with a WD and a main-sequence star, Zorotovic et al. (2010) suggested that the CE efficiency should be in the range of 0.2–0.3. If we adopt a low efficiency of 0.3 instead of 1.0 in the BPS calculations, the obtained birthrates of incipient NS–helium star (NS–normal star) binaries will be decreased by a factor of ~ 0.6 (~ 0.8), and the corresponding ULX numbers will be reduced by a factor of ~ 0.3 (~ 0.6).

kick, resulting in an eccentric orbit or even disruption of the binary system. The kick velocities are assumed to obey the Maxwellian distributions with a dispersion of $\sigma = 40 \text{ km s}^{-1}$ (Dessart et al. 2006) for NSs formed from electron-capture SNe and $\sigma = 265 \text{ km s}^{-1}$ (Hobbs et al. 2005) for NSs formed from core-collapse SNe.

The initial parameters of the primordial binaries are taken as follows. The primary stars obey the initial mass function suggested by Kroupa et al. (1993), and the mass ratios of the secondary to the primary are drawn from a flat distribution between 0 and 1. The orbital separations are assumed to be uniform in the logarithm (Abt 1983). We assume the initial orbits of all binaries are circular, as shown by Hurley et al. (2002), the outcome of the interactions of systems with the same semilatus rectum is almost independent of eccentricity. We adopt a binary fraction of 0.5 for stars with initial masses below $10M_{\odot}$, otherwise we assume all massive stars are in binaries. The initial metallicity of stars is set to be 0.02. We take the star formation history of Milky Way-like galaxies into account, assuming a constant star formation rate of $3M_{\odot} \text{ yr}^{-1}$ over the past 10 Gyr period.

In Figure 1 we plot the birthrate distributions of incipient NS–normal star (top panels) and NS–helium star (bottom panels) binaries. The left and right panels correspond to the distributions of the donor mass and the orbital period, respectively. In each panel, the black and grey curves represent the differential and cumulative distributions, respectively. We can see that the total birthrate of incipient NS–normal star systems is $\sim 1.2 \times 10^{-4} \text{ yr}^{-1}$. Such incipient binaries tend to have eccentric orbits due to mass loss and kick during SN. For simplicity, we assume that they are quickly circularized by tidal torques with the orbital angular momentum conserved³. The corresponding orbital separation is then reduced by a factor of $(1 - e^2)$, where e is the eccentricity. It can be seen that the orbital period distribution has two peaks at ~ 2 and ~ 50 days, which reflects whether the evolution of the primordial binaries has experienced a CE phase. The incipient NS–helium star binaries, as the descendants of long-period NS–normal star systems that are followed by a CE phase⁴, have a lower birthrate of $\sim 4 \times 10^{-5} \text{ yr}^{-1}$. These binaries are mainly close systems in a circular orbit, most of them have orbital periods of $\lesssim 1$ day.

2.2. Evolution of NS XRBs

Based on the obtained results in Figure 1, we track the evolutionary paths of incipient NS binaries with the stellar evolution code *MESA* (version number 10398, Paxton et al. 2011, 2013, 2015). The NS is treated as a point mass and its initial mass is set to be $1.4M_{\odot}$. The initial chemical compositions are taken to be $X = 0.7$, $Y = 0.28$, $Z = 0.02$ for normal stars and $Y = 0.98$,

³ There is a caveat that this assumption is not valid for long-period (e.g., > 20 days) systems. But under this assumption, we need only to take into account the binary parameters of the donor masses and the orbital periods when simulating the subsequent evolution of the incipient NS–normal star binaries (see Section 2.2 below).

⁴ It was proposed that an ONe WD may collapse into an NS induced by mass accretion in originally WD–helium star binaries (Chen et al. 2011; Liu et al. 2018). This channel may also lead to the formation of the NS–helium star binaries, but is not considered in our calculations.

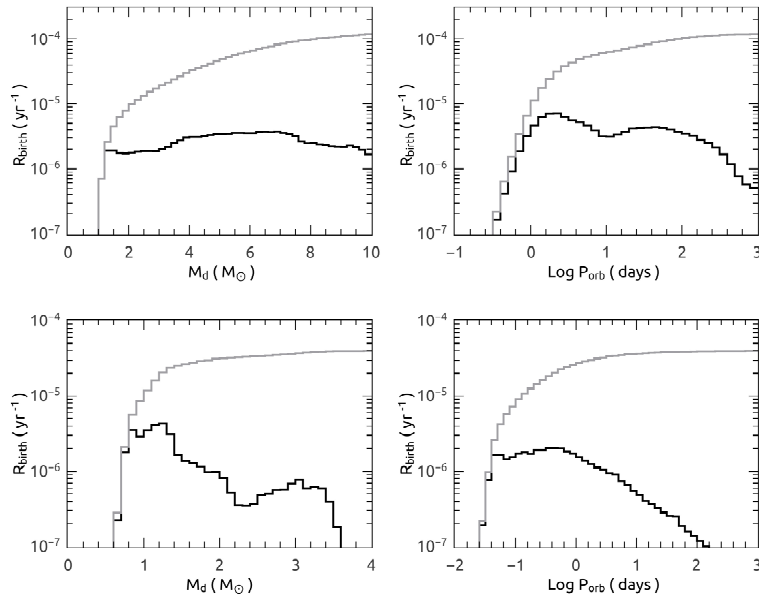


FIG. 1.— The birthrate distributions of the incipient NS binaries with a normal star (top panels) and a helium star (bottom panels) companion. The left and right panels depict the distributions of the donor mass and the orbital period, respectively. In each panel, the black and grey curves correspond to the differential and cumulative distributions, respectively.

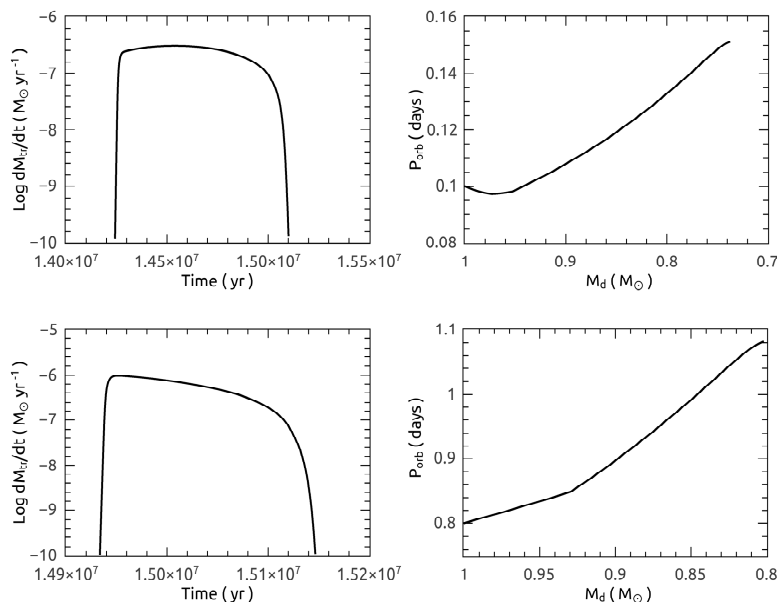


FIG. 2.— Exemplified evolution of the mass transfer rate (left panels) and the orbital period (right panels) for two typical NS–helium star binaries, as a function of the time and the donor mass. The initial masses of binary components are $M_{\text{NS}} = 1.4M_{\odot}$ and $M_{\text{d}} = 1.0M_{\odot}$. The top and bottom panels correspond to the initial orbital periods of 0.1 and 0.8 day, respectively.

$Z = 0.02$ for helium stars. Each incipient binary is characterized by the donor mass M_{d} and the orbital period P_{orb} . The incipient NS binaries from our BPS calculations are used to guide the limits of the *MESA* grid of initial binary parameters, thus we have evolved thousands of binary systems with different donor masses and orbital periods. For the NS–normal star systems, we vary the normal star masses from 1 to $10M_{\odot}^5$ by steps of $0.1M_{\odot}$

⁵ Note that the NS binaries with donor masses larger than $10M_{\odot}$ would have very small contribution to the ULX population in Milky Way-like galaxies (Shao & Li 2015).

and the orbital periods (in units of days) logarithmically from -0.5 to 3 by steps of 0.1 . For the NS–helium star systems, we increase the helium star masses from 0.6 to $4M_{\odot}$ by steps of $0.1M_{\odot}$ and the orbital periods (in units of days) logarithmically from -0.6 to 2 by steps of 0.1 . These binaries are used to represent all incipient NS binaries, the birthrate of a specific binary is obtained by summing the ones of the incipient binaries reside in the corresponding grid interval of $\Delta M_{\text{d}} \times \Delta(\log P_{\text{orb}})$.

During the evolution, we adopt the scheme of Ritter (1988) to compute the mass transfer rate via RLOF. We

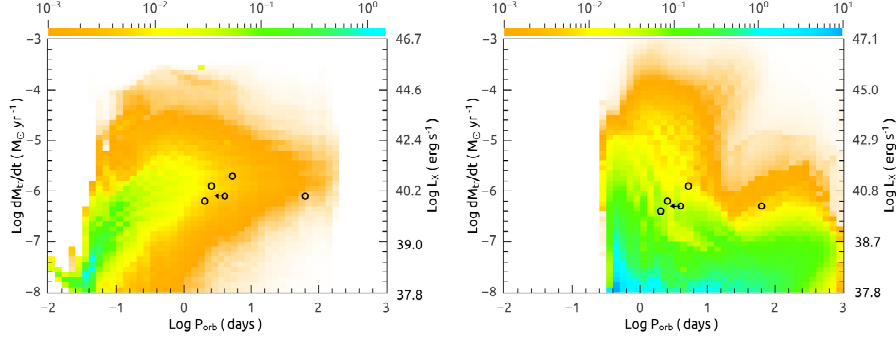


FIG. 3.— The number distributions of NS XRBs in the orbital period P_{orb} vs. mass transfer rate \dot{M}_{tr} plane, with the assumption of a constant star formation rate of $3M_{\odot}\text{yr}^{-1}$ over a period of 10 Gyr. The left and right panels correspond to the binaries containing a helium star and a normal star donor, respectively. Only the systems with mass transfer rates larger than $10^{-8}M_{\odot}\text{yr}^{-1}$ are presented, and the colors are scaled according to the number of the XRBs. The five black circles denote the observed NS ULXs with known orbital periods (see Table 1).

assume the mass increase onto an NS is limited by the Eddington accretion rate ($\sim 1.5 \times 10^{-8}M_{\odot}\text{yr}^{-1}$ for hydrogen accretion and $\sim 4 \times 10^{-8}M_{\odot}\text{yr}^{-1}$ for helium accretion). For the matter that is not accreted by the NS, we assume it escapes the binary system in the form of isotropic wind, taking away the NS’s specific orbital angular momentum. In some cases, the mass transfer rates rapidly increase to $\gtrsim 10^{-2}M_{\odot}\text{yr}^{-1}$, and the code fails to converge. These systems are expected to go into CE evolution soon. So we use this rate as a limited condition to judge whether the code is terminated. Whereas the ULX population are actually dominated by the binaries undergoing dynamically stable mass transfer with a modest rate of $\sim 10^{-7} - 10^{-6}M_{\odot}\text{yr}^{-1}$, the systems with extremely high mass transfer rates cannot significantly contribute the ULX systems (e.g., Shao & Li 2015).

For the NS–helium star binaries, the mass transfer takes place on the nuclear timescale if the initial helium stars are less massive than $\sim 2.0 - 2.5M_{\odot}$, otherwise the phase of mass transfer proceeds rapidly on the thermal timescale (see also Dewi et al. 2002). Hence the majority of the NS–helium star binaries obtained from our BPS calculations will experience a mass transfer phase that is driven by the nuclear evolutionary expansion of the helium stars. In Figure 2 we present the evolutionary tracks of two typical NS–helium star binaries as example. The initial systems contain a $1M_{\odot}$ helium star around the NS, and the orbital periods are chosen to be 0.1 (top panels) and 0.8 day (bottom panels). In the top panels, the beginning of RLOF occurs at the time of about 14.2 Myr. The mass transfer can persist over 0.7 Myr at a rate of $\gtrsim 10^{-7}M_{\odot}\text{yr}^{-1}$. After $0.26M_{\odot}$ of the envelope matter is transferred, the binary leaves an NS–WD system in a 0.15 day orbit. The final merger of this binary will happen in ~ 40 Myr later. In the bottom panels, the helium star evolves to fill its Roche lobe at the time of about 14.9 Myr. The mass transfer rapidly increases to $\sim 10^{-6}M_{\odot}\text{yr}^{-1}$ and then gradually decreases to $\sim 10^{-7}M_{\odot}\text{yr}^{-1}$ within a span of about 0.2 Myr. About $0.2M_{\odot}$ material is stripped during the mass transfer phase, the helium star turns into a massive WD of mass $\sim 0.8M_{\odot}$. The binary eventually becomes an NS–WD binary with the orbital period of 1.08 day, which is similar to a system like PSR B0655+64 (van den Heuvel & Taam 1984). It is obvious that the NS–helium

star binaries with typical initial parameters can spend a few tenths of Myr in the ULX phases.

Given the mass transfer rate \dot{M} in an XRB, the X-ray luminosity can be simply estimated with the traditional formula

$$L_{\text{X}} = 0.1\dot{M}c^2, \quad (1)$$

where c is the speed of light in vacuum. However, when \dot{M} is greater than the Eddington rate \dot{M}_{E} , the accretion disk becomes geometrically thick, which influences the X-ray luminosity. An NS that is being fed at a super-Eddington rate can shed more and more of the material as it approaches the NS along the disk, thereby never violating the Eddington limit locally. In this case, we follow King & Lasota (2016) to convert the mass transfer rate into the X-ray luminosity. The total accretion luminosity, by integrating the local disk emission (Shakura & Syunyaev 1973), is given as

$$L_{\text{acc}} \simeq L_{\text{E}} \left[1 + \ln \left(\frac{\dot{M}}{\dot{M}_{\text{E}}} \right) \right], \quad (2)$$

where L_{E} is the Eddington luminosity. With this equation, the binary system can emit an X-ray luminosity that is limited to a few times the Eddington limit. Due to the geometric collimation, one can see the source in directions within one of the radiation cones, with the apparent (isotropic) X-ray luminosity

$$L_{\text{X}} \simeq \frac{L_{\text{E}}}{b} \left[1 + \ln \left(\frac{\dot{M}}{\dot{M}_{\text{E}}} \right) \right], \quad (3)$$

where b is the beaming factor. King (2009) proposed an approximate formula

$$b \simeq \frac{73}{\dot{m}^2}, \quad (4)$$

where $\dot{m} = \dot{M}/\dot{M}_{\text{E}}$. This formula is valid for $\dot{m} \gtrsim 8.5$, otherwise the beaming effect is not operated (i.e., $b = 1$). Accordingly, we assume that the probability of detecting a source along the beam is reduced by a factor of b .

3. RESULTS AND DISCUSSIONS

In Figure 3 we plot the number distributions of the NS XRBs with a helium star (left panel) and a normal star

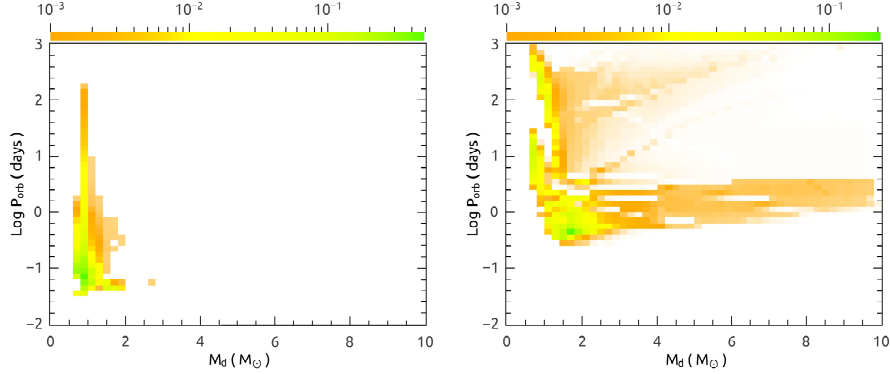


FIG. 4.— Expected number distributions of the NS ULXs containing a helium star (left panel) or a normal star (right panel) in the $M_d - P_{\text{orb}}$ plane. The colors are scaled according to the number of the ULX systems.

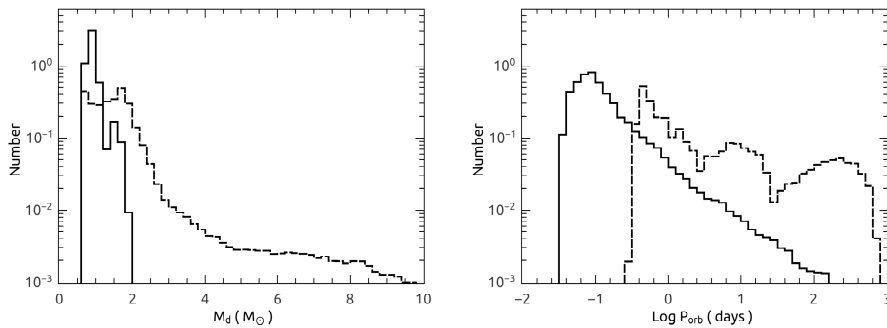


FIG. 5.— Expected number distributions of the NS ULXs as a function of the donor mass (left panel) and the orbital period (right panel). The solid and dashed curves denote the ULX systems containing a helium star and a normal star donor, respectively.

donor (right panel) in the orbital period–mass transfer rate ($P_{\text{orb}} - \dot{M}_{\text{tr}}$) plane. Only the systems with mass transfer rates larger than $10^{-8} M_{\odot} \text{yr}^{-1}$ are presented. According to the mass transfer rates labelled on the left side axis of each panel, we can calculate the corresponding apparent X-ray luminosities by considering possible beaming effect, which are labelled on the right side axis for comparison. Note that the calculated X-ray luminosities between the left and right panels have a slight difference, as the Eddington limits for helium and hydrogen accretion are differently adopted. The five black circles show the positions of the observed NS ULXs with known orbital periods (see Table 1). Each panel contains a 50×50 image matrix, the colors are scaled according to the number of the XRBs. After recording the evolutionary tracks of all NS binaries, we can calculate the number of binary systems passing through a specific matrix element by accumulating the product of their birthrates and the durations. We obtain that the NS XRBs with a helium star companion have the number of ~ 23 in a Milky Way-like galaxy, the ages of such systems are typically $\sim 100\text{Myr}$. It can be seen that only a small group (~ 9) of them can appear as ULXs because a high mass transfer rate of $\gtrsim 10^{-7} M_{\odot} \text{yr}^{-1}$ is required (King et al. 2017). When comparing these two diagrams, the calculated number distribution of the NS–normal star binaries seems to match the observations much better than the one of the NS–helium star binaries. It should be noted that, however, the observed sample of the NS ULXs is still too small and subject to the observational

bias that favoring luminous massive stars. In addition, the NSs in many ULX systems are likely to be unpulsed unless having high spin-up rates (King et al. 2017). It is unclear that whether the NS–helium star ULXs can be easily identified due to the emission of X-ray pulsations.

Figure 4 depicts the number distributions of the NS ULXs with X-ray luminosities greater than 10^{39}ergs^{-1} in the $M_d - P_{\text{orb}}$ plane. The effect of geometric beaming on detection probability is taken into account. The left and right panels correspond to the NS ULXs with a helium star and a normal star (see also Shao & Li 2015) companion, respectively. Also plotted in Figure 5 is the histogram distributions of the ULX numbers as a function of the donor mass and the orbital period. The solid and dashed curves respectively correspond to the NS ULXs with a helium star and a normal star donor. We find that the majority of the ULX systems containing a helium star donor are close systems with orbital periods distributing at a peak of ~ 0.1 day (with a tail up to ~ 100 days), and the mass distribution of the helium stars has a maximum probability at $\sim 1M_{\odot}$ within the whole range of $\sim 0.6 - 2M_{\odot}$. This is apparent because the helium stars in short-period systems are less evolved and possess longer durations of mass transfer phases. The systems with a massive ($\gtrsim 2M_{\odot}$) helium star are hardly produced because of a combination of relatively low birthrates, short mass transfer durations and low detection possibilities (due to the beaming effect).

Figure 6 presents the color-magnitude diagrams for the donors of the NS ULXs. The left and right panels correspond to the distributions of the helium star and the

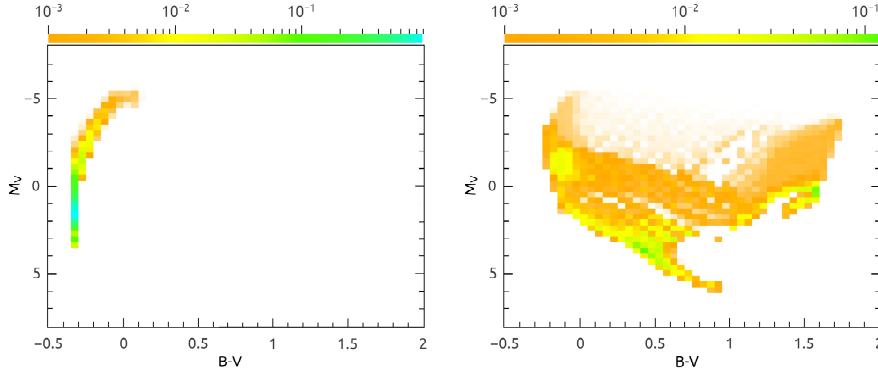


FIG. 6.— Color-magnitude diagrams for the donors in the NS ULXs. The left and right panels correspond to the distributions of the helium star and the normal star donors, respectively. The colors are scaled according to the number of the ULX systems.

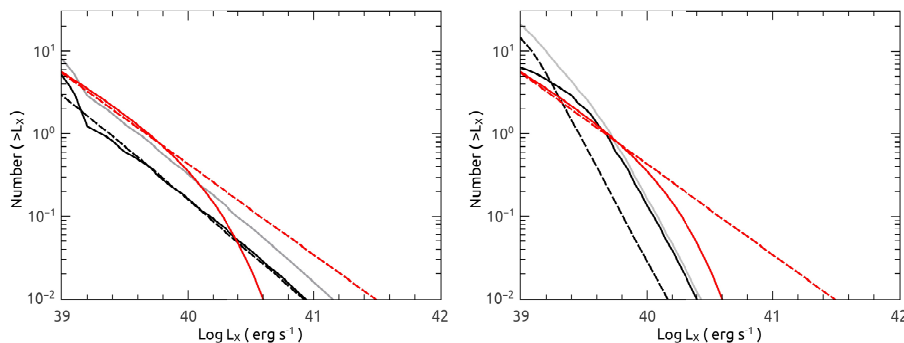


FIG. 7.— Expected numbers of NS ULXs at the present epoch as a function of X-ray luminosity in Milky Way-like galaxies with a constant star formation rate of $3M_{\odot} \text{ yr}^{-1}$. The left and right panels correspond to the cases when adopting Equations (3) and (1) to calculate the X-ray luminosity. In each panel, the black solid and black dashed curves respectively correspond to the ULX systems with a helium star and a normal star companion, and the grey solid curve corresponds to the whole population of the NS ULXs. Based on the observed ULX sample in nearby galaxies, the luminosity functions are fitted when applying two models of a power-law with an exponential cut-off (red solid curve) and a pure power-law (red dashed curve). Here the fit parameters are taken from Swartz et al. (2011).

normal star donors, respectively. In both cases, the majority of the ULX systems tend to have donors with absolute magnitude M_V larger than -1 magnitude, since the donors are predominantly low-mass ($\lesssim 2M_{\odot}$) stars as mentioned above. If located in external galaxies, the donor counterparts are probably too dim to be detected. Furthermore the optical emission from the donor star in a ULX system may be confused with that from the accretion disk around the compact star (Tao et al. 2011). Our results suggest that the characteristic of very short orbital periods can be used to distinguish the NS ULXs with a helium star donor.

In Figure 7 we show the X-ray luminosity function of the NS ULX population in Milky Way-like galaxies. The black solid and black dashed curves respectively correspond to the ULXs with a helium star and a normal star companion, and the grey solid curve corresponds to the whole population of the NS ULXs. The red curves present the fitted luminosity functions of the observed ULX sample in nearby galaxies (for details see Swartz et al. 2011). Note that these fitted luminosity functions have been normalized to a star formation rate of $3M_{\odot} \text{ yr}^{-1}$. In the left panel, the luminosity function for the ULX systems with a helium star donor has an obvious break at the position of $L_X \sim 2 \times 10^{39} \text{ erg s}^{-1}$, which corresponds to a point that the beaming effect starts operating. For the NS ULXs with a normal star

donor, the corresponding luminosity function also has a similar break but at $L_X \sim 6 \times 10^{38} \text{ erg s}^{-1}$, which is not covered in this diagram. In the right panel, we show the X-ray luminosity function without considering the beaming effect for comparison, by use of Equation (1) to calculate the X-ray luminosity. We expect that the NS–helium star systems can contribute several ULXs in a Milky Way-like galaxy, which is comparable with that from the NS–normal star binaries. The number of the extremely luminous sources with $L_X \geq 10^{40} \text{ erg s}^{-1}$ is only about ~ 0.3 . Although the ULX systems with a BH accretor are not included, our obtained number of the NS ULXs seems to match the observations.

Recently Wiktorowicz et al. (2017) performed a BPS study on the origin of the ULX systems, the NS–helium star binaries were also included in their calculations. The NS–helium star binaries could only appear as the extremely luminous sources, and they were expected to be very rare. At solar metallicity, the corresponding masses of the helium stars were in the range of $1.7 - 2.6M_{\odot}$ (Wiktorowicz et al. 2017). This mass range is significantly larger than the one ($\sim 0.6 - 2.0M_{\odot}$) obtained by us, since we adopt the rotation-dependent (highly non-conservative) mass transfer model during the primordial binary evolution. This model allows a large amount of the primordial binaries to experience stable mass transfer, and then evolve to be relatively wide systems con-

taining an NS and an intermediate-mass ($\sim 3 - 8M_{\odot}$) normal star (Shao & Li 2014). The subsequent evolution of these wide binaries is expected to go into a CE phase when the intermediate-mass donor starts transferring mass to the NS. After the CE evolution, the NS's companion may be a relatively low mass helium star. It is pointed out that a fraction of close binaries containing a (partially) recycled pulsar and a CO WD (with mass of $\sim 0.6 - 1.3M_{\odot}$) in the Milky Way are likely formed through this channel involving a CE phase (Tauris 2011). If so, our results that involve relatively low mass helium stars can better reproduce the observed binaries containing a relatively light ($\lesssim 1M_{\odot}$) CO WD.

4. SUMMARY

With a population synthesis study, we have shown that NS XRBs containing a helium star companion have a significant contribution to the ULX population in Milky Way-like galaxies. Assuming a constant star formation rate of $3M_{\odot}\text{yr}^{-1}$, we predict that there are several NS–helium star ULX systems in a Milky Way-like galaxy, whose ages are typically ~ 100 Myr. These ULX systems favor short orbital periods, so their subsequent evolution will lead to the formation of close NS–WD binaries which are important gravitational wave sources.

We thank the referee for useful suggestions to improve this paper. This work was supported by the Natural Science Foundation of China (Nos. 11973026, 11603010, 11773015, and 11563003) and Project U1838201 supported by NSFC and CAS, and the National Program on Key Research and Development Project (Grant No. 2016YFA0400803).

REFERENCES

- Abt, H. A. 1983, *ARA&A*, 21, 343
 Bachetti, M., Harrison, F. A., Walton, D. J., et al. 2014, *Nature*, 514, 202
 Begelman, M., 2002, *ApJ*, 568, 97
 Bhattacharya, D., & van den Heuvel, E. P. J. 1991, *PhRv*, 203, 1
 Binder, B., Levesque, E. M., & Dorn-Wallenstein, T. 2018, *ApJ*, 863, 141
 Brightman, M., Harrison, F. A., Fürst, F., et al. 2018, *Nature Astronomy*, 2, 312
 Carpano, S., Haberl, F., Maitra, C., & Vasilopoulos, G. 2018, *MNRAS*, 476, L45
 Chen W. C., Li X.-D., & Xu R. X., 2011, *A&A*, 530, A104
 Chen, W.-C. 2017, *MNRAS*, 465, L6
 Colbert, E., & Mushotzky, R. 1999, *ApJ*, 519, 89
 Dall’Osso, S., Perna, R., & Stella, L. 2015, *MNRAS*, 449, 2144
 de Mink, S. E., Pols, O. R., Langer, N., & Izzard, R. G. 2009, *A&A*, 507, L1
 de Mink, S. E., Langer, N., Izzard, R. G., Sana, H., & de Koter, A. 2013, *ApJ*, 764, 166
 Dessart, L., Burrows, A., Ott, C. D., et al. 2006, *ApJ*, 644, 1063
 Dewi, J. D. M., & Tauris, T. M., 2000, *A&A* 360, 1043
 Dewi, J. D. M., Pols, O. R., Savonije, G. J., & van den Heuvel, E. P. J. 2002, *MNRAS*, 331, 1027
 Doroshenko, V., Tsygankov, S., & Santangelo, A., 2018, *A&A*, 613, A19
 Ekşi, K. Y., Andaç, İ. C., Çikintoğlu, S., et al. 2015, *MNRAS*, 448, L40
 Farrell, S. A., Webb, N. A., Barret, D., Godet, O., Rodrigues, J. M. 2009, *Nature*, 460, 73
 Fragos, T., Linden, T., Kalogera, V., & Sklias, P. 2015, *ApJL*, 802, L5
 Fryer, C., Belczynski, K., Wiktorowicz, G., et al. 2012, *ApJ*, 749, 91
 Fürst, F., Walton, D. J., Harrison, F. A., et al. 2016, *ApJL*, 831, L14
 Gladstone, J. C., Roberts, T. P., & Done, C. 2009, *MNRAS*, 397, 1836
 Gladstone, J. C., Copperwheat, C., Heinke, C. O., et al. 2013, *ApJS*, 206, 14
 Heida, M., Jonker, P. G., Torres, M. A. P., et al. 2014, *MNRAS*, 442, 1054
 Heida, M., Harrison, F. A., Brightman, M. et al. 2019, *ApJ*, 871, 231
 Hobbs, G., Lorimer, D. R., Lyne, A. G., & Kramer, M. 2005, *MNRAS*, 360, 974
 Hurley, J. R., Pols, O. R., & Tout, C. A. 2000, *MNRAS*, 315, 543
 Hurley, J. R., Tout, C. A., & Pols, O. R. 2002, *MNRAS*, 329, 897
 Israel, G. L., Papitto, A., Esposito, P., et al. 2017a, *MNRAS*, 466, L48
 Israel, G. L., Belfiore, A., Stella, L., et al. 2017b, *Science*, 355, 817
 Ivanova, N., Justham, S., Chen, X., et al. 2013, *A&AR*, 21, 59
 Kaaret, P., Feng, H., & Roberts, T. P. 2017, *ARA&A*, 55, 303
 Karino, S., & Miller, J. C. 2016, *MNRAS*, 462, 3476
 King, A. R., Davies, M. B., Ward, M. J., Fabbiano, G., & Elvis, M. 2001, *ApJ*, 552, L109
 King A. R., 2009, *MNRAS*, 393, L41
 King A. R., & Lasota, J.-P. 2016, *MNRAS*, 458, L10
 King A. R., Lasota, J.-P., & Kluniak, W. 2017, *MNRAS*, 468, L59
 Kluzniak, W., & Lasota, J.-P. 2015, *MNRAS*, 448, L43
 Kolb, U., Davies, M. B., King, A., & Ritter, H. 2000, *MNRAS*, 317, 438
 Kroupa, P., Tout, C. A., & Gilmore, G. 1993, *MNRAS*, 262, 545
 Liu D., Wang B., Chen W., Zuo Z., & Han Z., 2018, *MNRAS*, 477, 384
 Liu, J., Bregman, J. N., Bai, Y., Justham, S. & Crowther, P. 2013, *Nature*, 503, 500
 Motch, C., Pakull, M. W., Soria, R., Gris, F., & Pietrzycki, G. 2014, *Nature*, 514, 198
 Nelson, C. A. & Eggleton, P. P. 2001, *ApJ*, 552, 664
 Packet, W. 1981, *A&A*, 102, 17
 Pasham, D. R., Strohmayer, T. E., Mushotzky, R. F. 2014, *Nature*, 513, 74
 Paxton, B., Bildsten, L., Dotter, A., et al. 2011, *ApJS*, 192, 3
 Paxton, B., Cantiello, M., Arras, P., et al. 2013, *ApJS*, 208, 4
 Paxton, B., Marchant, P., Schwab, J., et al. 2015, *ApJS*, 220, 15
 Petrovic, J., Langer, N., & van der Hucht, K. A. 2005, *A&A*, 435, 1013
 Podsiadlowski, P., & Rappaport, S. A., 2000, *ApJ*, 529, 946
 Podsiadlowski, Ph., Rappaport, S., & Pfahl, E. D. 2002, *ApJ*, 565, 1107
 Podsiadlowski, P., Langer, N., Poelarends, A. J. T., et al. 2004, *ApJ*, 612, 1044
 Poutanen, J., Lipunova, G., Fabrika, S., Butkevich, A. G., & Abolmasov, P. 2007, *MNRAS*, 377, 1187
 Ritter, H. 1988, *A&A*, 202, 93
 Roberts, T. P., Levan, A. J., & Goad, M. R. 2008, *MNRAS*, 387, 73
 Rodríguez Castillo, G. A., Israel, G. L., Belfiore, A. et al. 2019, arXiv: 1906.04791
 Sathyaprakash, R., Roberts, T. P., Walton, D. J. et al. 2019, *MNRAS*, 488, L35
 Shakura, N. I., & Syunyaev, R. A. 1973, *A&A*, 24, 337
 Shao, Y., & Li, X.-D. 2012, *ApJ*, 756, 85
 Shao, Y., & Li, X.-D. 2014, *ApJ*, 796, 37
 Shao, Y., & Li, X.-D. 2015, *ApJ*, 802, 131
 Shao, Y., & Li, X.-D. 2016, *ApJ*, 833, 108
 Shao, Y., & Li, X.-D. 2018, *ApJ*, 867, 124
 Stancliffe, R., & Eldridge, J. 2009, *MNRAS*, 396, 1699
 Sutton, A. D., Roberts, T. P., & Middleton, M. J. 2013, *MNRAS*, 435, 1758
 Swartz, D., Soria, R., Tennant, A., & Yukita, M. 2011, *ApJ*, 741, 49
 Tao, L., Feng, H., Grisé, F., & Kaaret, P. 2011, *ApJ*, 737, 81

- Tauris, T. M., van den Heuvel, E. P. J., & Savonije, G. J. 2000, *ApJ*, 530, L93
- Tauris, T. M. 2011, in *Evolution of Compact Binaries*, eds. L. Schmidtbreick, M. R. Schreiber, & C. Tappert, ASP Conf. Ser., 447, 285
- Tauris, T., Langer, N., & Podsiadlowski, P. 2015, *MNRAS*, 451, 2123
- Tong, H. 2015, *RAA*, 15, 517
- Tsygankov, S. S., Mushtukov, A. A., Suleimanov, V. F., & Poutanen, J. 2016, *MNRAS*, 457, 1101
- Tsygankov, S. S., Doroshenko, V., Lutovinov, A. A., Mushtukov, A. A., & Poutanen, J. 2017, *A&A*, 605, A39
- van den Heuvel, E. P. J., & Taam, R. 1984, *Nature*, 309, 235
- Vink, J. S., de Koter, A., & Lamers, H. J. G. L. M. 2001, *A&A*, 369, 574
- Walton, D. J., Fürst, F., Heida, M., et al. 2018, *ApJ*, 856, 128
- Wang, C., Jia, K., & Li, X.-D. 2016, *RAA*, 16, 126
- Webbink, R. F. 1984, *ApJ*, 277, 355
- Weng, S.-S., Ge, M.-Y., Zhao, H.-H., et al. 2017, *ApJ*, 843, 69
- Wiktorowicz, G., Sobolewska, M., Sdowski, A., & Belczynski, K. 2015, *ApJ*, 810, 20
- Wiktorowicz, G., Sobolewska, M., Lasota, J.-P., & Belczynski, K. 2017, *ApJ*, 846, 17
- Xu, K. & Li, X.-D. 2017, *ApJ*, 838, 98
- Xu, X.-J., & Li, X.-D. 2010, *ApJ*, 716, 114
- Zorotovic, M., Schreiber, M. R., Gänsicke, B. T., & Nebot Gómez-Morán, A. 2010, *A&A*, 520, 86